Chapter 10
The Early Phases of Epileptogenesis Induced by Status Epilepticus Are Characterized by Persistent Dynamical Regime of Intermittency Type

Massimo Rizzi, Federica Frigerio and Valentina Iori

Abstract Pre-clinical studies aimed to test potential anti-epileptogenic therapies by using the animal models of epileptogenesis induced by status epilepticus (SE), highlighted that the early days following the end of this primary insult represent a crucial temporal window for the subsequent development of epilepsy. In this study, we characterized the EEG dynamics during such crucial period of epileptogenesis, according to the conceptual framework of nonlinear dynamical systems. To this aim, we analyzed by recurrence quantification analysis (RQA) the EEG signals associated to the early days of epileptogenesis induced by SE in rodents according to two well-known experimental protocols, i.e., (i) SE induced by electrical stimulation of the hippocampus in rats (n = 7) and (ii) SE induced by the intra-amygdala administration of kainic-acid in mice (n = 6). We show that the EEG signals during the early 1–2 days post-SE are characterized by an enhanced and persistent rate of occurrence of dynamical regimes of intermittency type. This finding is common to both models of SE, hence it could represent the dynamical hallmark of pro-epileptogenic insults and could correlate with the efficacy of such insults to promote functional changes leading to the development of epilepsy. Future works aimed to deepen our findings could lead to the identification of a potential prognostic factor of the development of epilepsy as well as improve the portability of pre-clinical studies aimed to target new potential therapeutics designed to prevent the development of epilepsy.

10.1 Introduction

Brain insults as, for instance, traumatic brain injury, stroke or infectious diseases, are known as risk factors for the development of epilepsy and the prevention of this neurological disorder in individuals at risk still represents an important medical

M. Rizzi (✉) · F. Frigerio · V. Iori
Department of Neuroscience, IRCCS—Istituto di Ricerche
Farmacologiche Mario Negri, Via La Masa 19, 20156 Milan, Italy
e-mail: massimo.rizzi@marionegri.it; massimo.rizzi@gmail.com

185

challenge. In this context, the term epileptogenesis (or latent period) is referred to as the period which elapses between the occurrence of a pro-epileptogenic insult and the emergence of the first spontaneous seizure. Pre-clinical studies accomplished by using several animal models of epileptogenesis have highlighted the occurrence of many cellular and functional alterations in the brain tissue. Among these alterations, to name a few, the neurodegeneration of brain tissue and the reorganization of the molecular architecture of individual neurons, as well as alterations of the blood-brain barrier permeability and the alteration of patterns of expression of molecules related to the immune response [1]. Targeting of some of these pathological mechanisms has shown favorable effects on the development of epileptogenesis in clinical studies (for a comprehensive review see [2], and references there in), pointing out that all cases of potential antiepileptogenic therapies which show a beneficial effect are to be administered during the early days of the latent period, often soon after the end of the primary insult [2]. This bulk of evidence strongly suggests that the very early days following the induction of a pro-epileptogenic insult represent a crucial time window for the development of epilepsy.

Many efforts are currently aimed to investigate on the potentially epileptogenic cellular and functional alterations occurring during such crucial early phases of epileptogenesis. However, much less effort is aimed to characterize the brain electrical activity which subtend the EEG during the same period. It cannot be underestimated that the characterization of the nature of the dynamics of the EEG activity during the latent period may contribute to shed light on the mechanisms of epileptogenesis as well as suggest new strategies of therapeutic intervention aimed to prevent the development of epilepsy. Accordingly, in this study we characterized the EEG dynamics occurring during the early phases of epileptogenesis, according to the paradigm of nonlinear dynamical systems. To this aim, we analysed the EEG signals associated to two well-known experimental models of status epilepticus (SE) induced in rodents, i.e., SE induced by the electrical stimulation of the hippocampus in rats and SE induced by intra-amygdala administration of kainic-acid in mice. As analytical method we specifically choose the recurrence quantification analysis [3], a valuable mathematical tool, aimed to efficiently characterize the nonlinear dynamics embedded in short, noisy and nonstationary time-series, being the latter two features intrinsically associated to the nature of EEG signals [3–5]. In the context of epilepsy, several research groups have already applied the RQA to analyse EEG signals, gaining intriguing results (for a reliable and updated survey of the state-of-the art of the application of the RQA to epileptic EEGs, see http://www. recurrence-plot.tk/bibliography.php). Nonetheless, one notices that all the available studies were aimed to predict/detect the occurrence of seizures or classify epileptic EEG patterns in cases of overt epilepsy in humans or following acute seizures induced in experimental animals. At present, despite the growing importance of the experimental models of SE in the epilepsy research, the characterization of nonlinear EEG dynamics during the development of epileptogenesis is lacking. Therefore, the application of the RQA to investigate the EEG dynamics during the early phases of epileptogenesis can be reasonably considered not only as a novelty per se but also as a necessity to better characterize these models.

10.2   Methods

10.2.1   Animals

Male Sprague-Dawley rats (275–300 g; Charles-River, Calco, Italy; n = 7) and male C57BL6N mice (~20 g; Charles-River, Calco, Italy; n = 6) were maintained in SPF facilities at the Mario Negri Institute and housed at a constant room temperature (23 °C) and relative humidity (60 ± 5 %) with free access to food and water and a fixed 12 h light/dark cycle.

10.2.2   Models of Epileptogenesis

A major contribution to the understanding of mechanisms involved in epileptogenesis comes from animal models where the primary pro-epileptogenic insult is the status epilepticus (SE) [6, 7]. SE is a condition defined as a seizure that persists for at least 5–10 min, or it repeats itself frequently enough so that there is not a resolution of contiguity [8]. In humans, SE may occur in association with different forms of brain injury and conditions such as stroke, brain trauma, withdrawal of anti-epileptic drug treatment and exposure to toxic nerve agents. As an experimental model of epileptogenesis, SE is commonly induced in rodents by electrical stimulation of specific brain areas or by the systemic or local administration of convulsive drugs [2, 6, 7, 9, 10]. In this work, we exploited the EEG signals originated from two well-known experimental models of SE, i.e., SE induced by the electrical stimulation of the hippocampus in rats [11, 12] and SE induced by intra-amygdala administration of kainic-acid in mice [13, 14].

The following experimental procedures were conducted in conformity with institutional guidelines that are in compliance with national (D.L. n.26, G.U. March 4, 2014) and international guidelines and laws (EEC Council Directive 86/609, OJ L 358, 1, December 12, 1987, Guide for the Care and Use of Laboratory Animals, U.S. National Research Council, 1996), and were reviewed and approved by the intramural ethical committee.

10.2.2.1   Surgical Procedure and Induction of the SE for the Rat Model of Epileptogenesis

Rats were surgically implanted under 1.5 % isoflurane anesthesia with 2 bipolar Teflon-insulated stainless-steel depth electrodes placed bilaterally into the temporal pole of the hippocampus (from bregma, mm: AP − 4.7; L ± 5.0; −5.0 below dura, [15]). Two screw electrodes were positioned over the nasal sinus and the cerebellum, and used as ground and reference electrodes, respectively. Electrodes were connected to a multipin socket and secured to the skull by acrylic dental cement. After surgical

procedures, rats were treated locally with Cicatrene powder (Neomicyn; Bacitracin; Glicyne; L-Cistein; DL-Treonin) and injected with Ampicillin (100 mg/kg, s.c.) for 4 days to prevent infections. Rats were allowed to recover from surgery in their home cage for 7–10 days. Before electrical stimulation, EEG baseline hippocampal activity was recorded in freely-moving rats for 24 h. Then, rats were unilaterally stimulated (50 Hz, 400 µA peak-to-peak, 1 ms biphasic square waves in 10 s trains delivered every 11 s) in the CA3 region of the ventral hippocampus for 90 min to induce SE according to a well-established protocol [11, 12]. SE was defined as the presence of continuous spike activity with a frequency higher than 0.5 Hz intermixed with high amplitude and frequency discharges lasting for at least 5 s, with a frequency of ≥ 8 Hz and an amplitude twofold-higher than the baseline. Spikes were defined as sharp waves with amplitude of at least 2.5-fold higher than the baseline and duration lower than 100 ms, or as a spike-and-wave with duration lower than 200 ms [9]. The end of SE was determined by the occurrence of inter-spike interval >2 s. No pharmacological intervention was done to stop SE since no mortality is observed in this model. In order to ascertain the development of epilepsy according to this model of epileptogenesis, rats were continuously EEG recorded (24 h/day) from SE induction until 2 spontaneous EEG seizures occurred. EEG was recorded using the Twin EEG Recording System connected with a Comet AS-40 32/8 Amplifier (sampling rate 400 Hz, high-pass filter 0.3 Hz, low-pass filter 70 Hz, sensitivity 2000 mV/cm; Grass-Telefactor, West Warwick, R.I., U.S.A.)

For this model of epileptogenesis, we considered for nonlinear analysis, the EEG signal which originated from the hippocampal electrode used for the induction of the SE by electrical stimulation.

10.2.2.2 Surgical Procedure and Induction of the SE for the Mouse Model of Epileptogenesis

Mice were surgically implanted under general gas anesthesia (1–3 % isoflurane in O_2) and stereotaxic guidance. A 23-gauge cannula was unilaterally positioned on top of the *dura mater* for the intra-amygdala injection of kainic acid (from bregma, mm: nose bar 0; anteroposterior −1.06, lateral −2.75) [16]. A nichrome-insulated bipolar depth electrodes (60 µm OD) was implanted in the dorsal hippocampus ipsilateral to the injected amygdala (from bregma, mm: nose bar 0; anteroposterior −1.8, lateral 1.5 and 2.0 below dura mater) [16]. Additionally, a cortical electrode was implanted onto the somatosensory cortex in the contralateral hemisphere. Electrodes were connected to a multipin socket (PlasticOne Inc., USA). One week after surgery, mice were connected to the EEG set up and the SE was induced by the injection of kainic acid (0.3 µg in 0.2 µl) in the basolateral amygdala in freely moving mice using a needle protruding of 3.9 mm below the implanted cannula. SE developed after approximately 10 min from kainic acid injection, and was defined by the appearance of continuous spikes with a frequency >1.0 Hz. Spikes were defined as sharp waves with an amplitude at least 2.5-fold higher than the baseline and a duration of <20 ms, or as a spike-and-wave with a duration of <200 ms [17].

After 40 min from SE onset, mice received diazepam (10 mg/kg, ip) to improve their survival. SE lasted for 7.0 $\pm$ 1.0 h and its end was determined by the occurrence of inter-spike interval >2 s. In order to ascertain the development of epilepsy according to this model of epileptogenesis, mice were continuously EEG recorded (24 h/day) from SE induction until 2 spontaneous EEG seizures occurred. EEG was recorded using the Twin EEG Recording System connected with a Comet AS-40 32/8 Amplifier (sampling rate 400 Hz, high-pass filter 0.3 Hz, low-pass filter 70 Hz, sensitivity 2000 mV/cm; Grass-Telefactor, West Warwick, R.I., U.S.A.)

For this model of epileptogenesis, we considered for nonlinear analysis, the EEG signal which originated from the hippocampal electrode positioned ipsilaterally to the site of intra-amygdala administration of kainic-acid.

10.2.3   Selection Criteria of the Time Windows of Epileptogenesis and the Related EEG Epochs, for Nonlinear Analysis

The duration of the epileptogenesis was variable. For rats, which underwent the protocol of induction of SE by electrical stimulation of the hippocampus, the duration of the latent period ranged from 7 to 11 days (mean $\pm$ SD = 9.17 $\pm$ 1.60) whereas for mice, which underwent the protocol of induction of SE by the intra-amygdala injection of kainic-acid, ranged from 6 to 8 days (mean $\pm$ SD = 6.80 $\pm$ 0.84). However, we focused our attention on the early days of epileptogenesis, since they were shown as crucial for the development of epilepsy. Specifically, we evaluated EEG signals associated to the early 5 days of epileptogenesis for rats and the early 4 days of epileptogenesis for mice. This criterion allowed to evaluate comparable time windows of epileptogenesis between the two models of induction of SE. Indeed, for rats, the early 5 days of epileptogenesis corresponded to 55.99 $\pm$ 10.03 % (mean $\pm$ SD) of the total time of epileptogenesis, whereas for mice, the early 4 days of epileptogenesis corresponded to 59.52 $\pm$ 7.14 % (mean $\pm$ SD) of the total time of epileptogenesis. Additionally, in authors' opinion, these temporal windows were sufficiently far (at least 2 days) from the onset of the first seizure, thus reducing the risk of bias due to the possibility of the emergence of mechanisms leading to the onset of the first seizure.

The EEG signals associated to each day of the selected time windows, were sampled at 400 Hz and analog-to-digital converted with 12 bit precision. Respect to the original EEG recordings which were 0.3–70 Hz band-pass filtered, we further restricted the range of EEG frequencies according to evidence suggesting a more circumscribed frequency band (<50 Hz) as being more relevant to the aim of our investigation. Indeed, significant changes of the power spectral density of the EEG frequency bands, ranging from delta (1–4 Hz) to low-gamma frequency band (30–50 Hz), were shown to occur in cortical structures, as the hippocampus, during the early phases of epileptogenesis [18, 19]. These changes show a temporal profile

similar to that of cellular and functional alterations occurring in the brain during the latent period, and they correlate with the emergence of well-known comorbidities of epilepsy (e.g., spatial memory deficits and/or social behavioral dysfunctions), which were shown to develop during the early phases of epileptogenesis [18, 19]. Therefore, it is reasonable to expect that frequency bands below 50 Hz are those bearing the majority of information on EEG dynamics during the early phases of epileptogenesis. Accordingly, also considering the electrical noise due to the frequency of the power grid (50 Hz), we applied a low-pass 50 Hz filter to all EEG recordings. These recordings were also visually inspected for removal of evident gross artifacts, if any. Successively, in the time interval from 01:00 pm to 07:00 pm, we extracted 12-s epochs (i.e. 4800 data points) every 10 min of each EEG signal. For rats, the same procedure was applied also to basal EEG recordings obtained before the induction of the SE, whereas for mice there were no basal EEG recordings available. We chose the time interval from 01:00 pm to 07:00 pm since the ordinary tiding up of the animal housings is usually accomplished in the morning and the light/dark cycle switches from one state to the other at 07:00 am/pm, respectively. Therefore, we decided to extract EEG epochs during this period in order to minimize the potential effects of environmental stress and variation of circadian rhythms on the EEG dynamics of the animals. Each epoch was then analyzed by the recurrence quantification analysis.

10.2.4 The Recurrence Quantification Analysis

All the possible states of a nonlinear dynamical system are usually represented as trajectories in the phase (or state) space, being a trajectory the depiction of the time evolution of a set of states of the system. A fundamental property of nonlinear dynamical systems is the recurrence of states, which are expected to become arbitrarily close to each other after a sufficient time [20]. By exploiting this property of dynamical systems, Eckmann and colleagues [21] introduced the technique of the Recurrence Plot (RP), which is a graphical representation of a square matrix, in which the matrix elements correspond to those times at which a state of a dynamical system recurs. Technically, the RP reveals all the times when the phase space trajectory of the dynamical system visits roughly the same area in the phase space [22] (see also www.recurrence-plot.tk). The RPs allow to represent any m-dimensional phase space trajectory through a two-dimensional plot of its recurrences, since each recurrence of a state at two different times is marked within the two-dimensional squared matrix according to a binary decision, e.g., ones and zeros (black and white dots in the plot) to denote if these two states are recurrent (one/black) or not (zero/white). From the graphical perspective, the RPs exhibit characteristic large scale and small scale patterns denoted by Eckmann et al. [21] as typology and texture, respectively. Importantly, the small scale structures of texture consist of single dots, diagonal lines as well as vertical and horizontal lines. Single, isolated recurrence points can occur if states are rare and can be due to chance or

noise. A diagonal line occurs when a segment of the trajectory is parallel to another segment, i.e. the trajectory visits the same region of the phase space at different times. The length of a diagonal line is determined by the duration of such similar local evolution of the trajectory segments and was shown to be inversely related to the extent of the Lyapunov exponent. A vertical (horizontal) line marks a time length in which a state does not change or changes very slowly, as in laminar states (intermittency).

As intended since their introduction, RPs allow the visual inspection of high dimensional phase space trajectories by giving hints about their time evolution even in case of short, noisy and nonstationary dataset. However, although important behavioral properties of dynamical systems can be qualitatively inferred from a visual inspection of RPs by a well-trained investigator, being RPs intrinsically a visualizing tool, their usefulness is nevertheless limited when one considers to exploit RPs extensively as analytical technique. Such limitation was totally removed by Zbilut and Webber [3] who introduced the Recurrence Quantification Analysis (RQA), a powerful analytical technique based on the mathematical defi-nition of variables introduced in order to measure some important properties of a nonlinear dynamical system by mean of an appropriate quantification of the small scale structures of the corresponding RP. At the present state of development of the RQA, several variables have been introduced [3, 23] (see also http://www.recurrence-plot.tk). In this work, we considered the variables which have been defined as follows:

- Recurrence Rate (REC), which represents the density of recurrence points in a RP. The recurrence rate corresponds with the probability that a specific state will recur and is expressed as

$$REC = \left(\frac{1}{N^2}\right) \sum_{i,j=1}^{N} R_{i,j} \qquad (10.1)$$

with $R_{i,j} = \Theta\,(RAD_i - \|\,x_i - x_j\|)$, $x_i \in \Re^m$, $i, j = 1 \ldots N$, where N is the number of considered states, x_i, RAD_i is a threshold distance (a.k.a. *radius*), $\|\cdot\|$ a norm and $\Theta(\cdot)$ the Heaviside function;

- Determinism (DET), which is the fraction of recurrence points forming diagonal lines. Diagonal lines represent epochs of similar time evolution of states of the system. Therefore, DET is related with the determinism of the system and is expressed as

$$DET = \frac{\sum_{l=l_{min}}^{N} lP(l)}{\sum_{l=1}^{N} lP(l)} \qquad (10.2)$$

where l is the diagonal line length considered when its value is $\geq l_{min}$ and $P(l)$ is the probability distribution of line lengths;

- Longest Diagonal Line (DMAX), which measures the dynamical stability of the system, being inversely related to the largest Lyapunov exponent

$$DMAX = max(\{l_i, i = 1, \ldots N_i\}) \tag{10.3}$$

- Shannon Entropy (ENT) of the distribution of the line lengths, which is a measure of the complexity of the recurrence structure

$$ENT = - \sum_{l=l_{min}}^{N} p(l) \ln p(l) \tag{10.4}$$

where $p(l) = P(l)/N_l$ is the probability to find a diagonal line of exactly length l in the RP, being N_l the total number of diagonal lines.

- Laminarity (LAM), which is the fraction of recurrence points forming vertical lines. Vertical lines represent unchanged or slowly changing states of the system and are associated to laminar states. LAM is defined as

$$LAM = \frac{\sum_{v=v_{min}}^{N} v P(v)}{\sum_{v=1}^{N} v P(v)} \tag{10.5}$$

where v is the vertical line length considered when its value is $\geq v_{min}$ and $P(v)$ is the probability distribution of vertical line lengths;

- Trapping time (TT), which represents the average length of the vertical lines

$$TT = \frac{\sum_{v=v_{min}}^{N} v P(v)}{\sum_{v=v_{min}}^{N} v P(v)} \tag{10.6}$$

- Longest Vertical Line (VMAX), which represents the length of the longest vertical line

$$VMAX = max(\{v_i, i = 1, \ldots, N_v\}) \tag{10.7}$$

The computation of RQA variables is based on the preliminary reconstruction of the trajectories of the system in a phase space. In the specific case of a univariate time series, as the EEG, such reconstruction is based on the so-called time delay-embedding procedure as introduced by Takens [24]. The exceptional usefulness of the Takens' theorem can be particularly appreciated in the fields of biomedicine and life sciences in that the variables determining the underlining dynamics of systems are often unknown, and time series of just one single

observable can be the only data available. According to the Takens' theorem, the topological features of any high-dimensional system consisting of multiple coupled variables can be reconstructed by measuring just a single variable of that system [24, 25]. In other words, a single observable of the system is sufficient to allow the reconstruction of the trajectories in a high-dimensional phase space. This phase space is different from the 'true' phase space, and the reconstructed trajectories do not preserve the geometric shape as they would have had in the 'true' phase space. However, the reconstructed phase space preserves the properties of the dynamical system, since they are unaffected by smooth coordinate changes (topological invariants). A major advantage of the Takens' theorem is in that the 'true' phase space of the system can be totally unknown, as it is often the case in the context of biological systems. A single point of a trajectory in a phase space reconstructed according to the Takens' theorem, represents a vector made of m time points selected from the time series, where two consecutive time points are delayed by a predetermined time lag (a.k.a. *time delay*). The number of time points (m) chosen as components of vectors is referred to as the *embedding dimension* of the time-series. Therefore, the reconstructed phase space has m-axis, one for each of the m components of the vector. Besides the embedding dimension and the time delay, RQA requires to set a threshold value, the *radius* (RAD), by which a state point embedded in the reconstructed phase space can be considered as being recurrent, as defined above, hence included in the recurrence matrix.

The embedding dimension, the RAD and, to a lesser extent, the time delay are the most important parameters for an accurate RQA and their determination is a crucial step. To this aim, we accomplished a preliminary scaling analysis of subsets of epochs, according to the strategy suggested by Webber and Zbilut [25]. Scaling analysis allows to determine sets of values of embedding dimension and RAD for which the nonlinear deterministic patterns (if any) of the time series under investigation are sufficiently unveiled. A significant deterministic pattern to consider as a reference for an appropriate choice of parameters is the exponential scaling behavior of the variable REC versus the variable RAD. This scaling behavior is graphically manifested as a linear tract on a log-log plot of REC versus RAD and is usually expected to occur at low percentage values of REC, typically from 0.05 to 2 %. However, we noticed that the common approach of choosing a fixed RAD and then to determine the RQA variables might not be the most appropriate method for the analysis of our EEG epochs. Indeed, the log-log plots of REC versus RAD may show a linear tract of variable extension. Therefore, a fixed RAD does not ensure that the percentage of REC is within the linear range of the log-log plot of REC versus RAD, being this condition a stringent requirement for an appropriate estimation of RQA variables [25]. Therefore, in our study, it was advisable to consider the RAD as a variable and the REC as a parameter that we set to 1 %, a percentage which assured a sparse recurrence matrix and the preservation of the linear relationship of log-log plot of REC versus RAD in all cases considered. Additionally, scaling analysis suggested as a good choice for the embedding dimension, any value ranging from 10 to 15, hence we choose 12. We decided to not set a time delay common to all epochs and to determine the appropriate time delay for each epoch by considering the first

local minima of the mutual information function. The value of the time delay was used also for the determination of the Theiler's window [26], that we calculated according to Gao [27], i.e., [(m − 1) * (time delay)], thus reducing the influence of tangential motion in the estimate of the RQA variables [23].

The recurrence matrix was normalized to the maximum distance [25] and the variable RAD was expressed as percentage of the recurrence matrix, whereas the distance between vectors was computed as Euclidean distance. Additionally, the minimum diagonal line length was set at a conservative value of 5, since the observational noise was shown to significantly affect the value of DET by increasing the amount of diagonal lines with spurious diagonal segments with length ≤4 [28]. The minimum vertical line length was set at the default value of 2, since there are no indications available on the effect of noise on this parameter.

10.2.5 Surrogates Technique and Test of Significance

The significance of each RQA variable was tested against the null hypothesis of being the expression of a Gaussian linear stochastic process. According to the surrogate data technique as introduced by Theiler [26, 29], and similarly to Ouyang and colleagues [30], for each 12-s EEG epoch, we generated 50 surrogate epochs by the technique of the inverse Fourier transform with phase randomization [29, 31], thus creating surrogate epochs which preserved the Fourier amplitude as well as the same distribution of values of the original epoch, with the exception that nonlinear determinism, if any, was disrupted. For each of the 50 surrogate epochs, the RQA variables were calculated and then the so-called Theiler's sigma (TS) was determined [26, 30] as follows:

$$TS = \frac{\left| VAR_{orig} - \overline{VAR_{surr}} \right|}{SD\left(VAR_{surr}^{i}\right)} \tag{10.8}$$

where VAR_{orig} refers to any RQA variable (*RAD, DET, LAM*, etc.…) calculated for the original EEG epoch, and $\overline{VAR_{surr}}$ and $SD\left(VAR_{surr}^{i}\right)$ refer to the mean and the standard deviation of the same variable as calculated considering the 50 surrogates created from that original EEG epoch. For any RQA variable, when its corresponding value of TS > 1.96, the amplitude of that variable reflects actual nonlinear processes occurring in the original EEG epoch. In this work, only RQA variables which passed the TS test were considered.

10.2.6 Computational Resources and Software

The time for calculation of the RQA variables was considerably shortened by the High-Throughput-Computing Technology, a.k.a. Grid Computing Technology [32].

A Grid infrastructure represents a network of geographically-distributed computational resources which allow scientific communities to develop applications to be executed on distributed computational and storage resources across the Internet. The computational resources used in this study were those of the Italian e-Infrastructure of the INFN (National Institute of Nuclear Physics), which is part of the Italian Grid Infrastructure (IGI) that is fully integrated in the EGI project (European Grid Infrastructure), the Europe's leading grid computing infrastructure co-funded by the EU in the context of the 6th and 7th Framework Program. The middleware, i.e., the software specifically developed to manage the workload across the distributed computational and storage resources of a grid infrastructure, was gLite v. 3.1-3.2 and the interactive sessions were made by a Scientific-Linux command-line interface.

In this study the RQA was accomplished by the applications RQS and RQH, as developed by Webber [33] (freely available for Windows operating systems at http://homepages.luc.edu/~cwebber). However, in order to implement the Theiler's window and to make the applications executable in the Grid Computing environment, the applications RQS and RQH were adapted with minor modifications as ANSI C code. The applications for the calculation of the time delay as well as for construction of surrogates were *mutual, minima, extrema* and *surrogates*, available in the TISEAN software package [34] (freely available at http://www.mpipks-dresden.mpg.de/~tisean).

10.2.7 Statistics

Statistical tests were performed by the software package GraphPad Prism 6 (GraphPad Software Inc., San Diego, California, USA). The great majority of datasets did not passed the test for normality according to the D'Agostino and Pearson omnibus test for normality as well as the Shapiro-Wilk normality test in case of small datasets ($P < 0.05$). Therefore, we used the nonparametric Kruskal-Wallis test, followed by Dunn's multiple comparisons test, in case of significant variation of medians. For graphical purposes, datasets were represented by the descriptive statistics mean $\pm$ SEM.

10.3 Results

Results are organized in figures and tables so that for each figure representing the trends of specific RQA metrics the related statistics are reported in the table labeled with the same progressive number (e.g.: for metrics represented in Fig. 10.1 the related statistics are reported in Table 10.1, and so on).
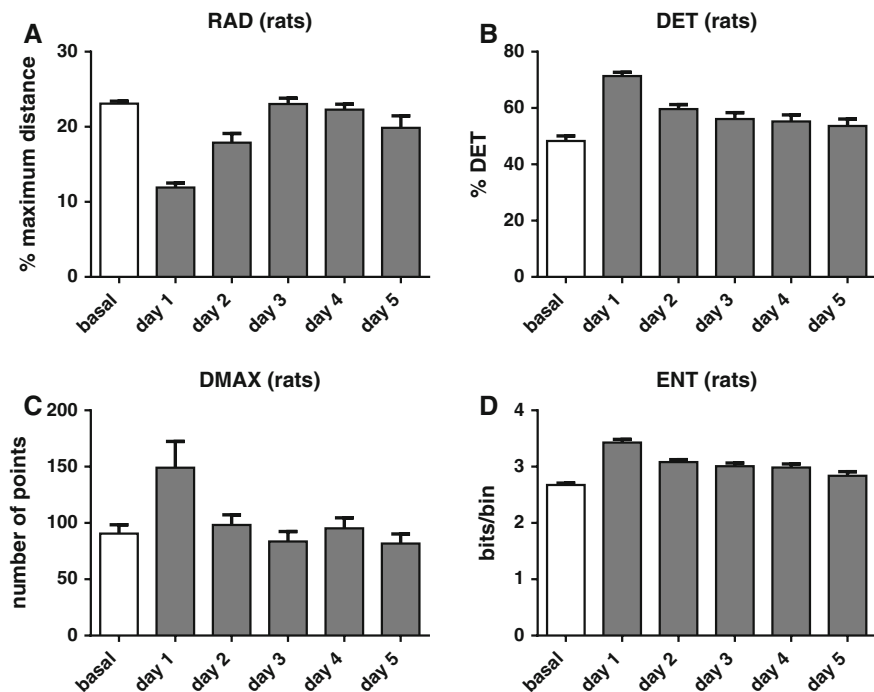
Fig. 10.1 Histograms (mean ± SEM) of datasets of RQA variables calculated in basal condition (*white bar*) and during the early 5 days of epileptogenesis (*grey bars*) for the model of SE induced in rats by the electrical stimulation of the hippocampus. *Panel A* depicts the variation of the variable RAD, whereas *panels B*, *C* and *D*, show how RQA metrics based on the *diagonal lines* of the RPs (DET, DMAX and ENT) are affected by the progression of epileptogenesis after the end of the primary insult

For both models of SE, the early 1–2 days of epileptogenesis are characterized by a significant reduction of the medians of the variable RAD (for rats, Fig. 10.1 panel A, $P < 0.0001$; for mice, Fig. 10.3 panel A, $P < 0.0001$—detailed statistics in Tables 10.1 and 10.3, respectively), thus suggesting an increased rate of recurrences during this time window, i.e., a higher density of the trajectories in the phase space of the system. Hence, a lower value of the variable RAD is sufficient to gain the percentage of recurrent points that we kept fixed at 1 % in order to assure the exponential scaling behavior of REC versus RAD, a basic requirement for a proper RQA [25].

The trends of the medians of the variables DET and LAM are reported in Figs. 10.1 (panel B) and 10.2 (panel A), for rats, whereas for mice are reported in Figs. 10.3 (panel B) and 10.4 (panel A). The detailed statistics for these metrics are reported in Tables 10.1 and 10.2 for rats and in Tables 10.3 and 10.4 for mice. The amount of DET significantly increases in the early 1–2 days post-SE for both models (for rats, Fig. 10.1 panel B, $P < 0.0001$; for mice, Fig. 10.3 panel B, $P = 0.0006$—Tables 10.1 and 10.3, respectively, for detailed statistics), whereas the amount of LAM shows opposite trends of variation (compare Fig. 10.2 panel A

Table 10.1 Nonparametric statistics (Kruskal-Wallis test, followed by Dunn's multiple comparisons test) of RQA metrics reported in Fig. 10.1

	RAD	DET	DMAX	ENT
Kruskal-Wallis test				
P value	<0.0001****	<0.0001****	0.0039**	<0.0001****
No of groups	6	6	6	6
No of values (total)	231	336	162	366
Kruskal-Wallis statistic	89.48	76.85	17.33	90.04
Dunn's multiple comparisons test				
Groups	*P value*	*P value*	*P value*	*P value*
Basal versus day 1	<0.0001****	<0.0001****	0.0074**	<0.0001****
Basal versus day 2	0.0054 **	0.0006 ***	ns	<0.0001****
Basal versus day 3	ns	ns	ns	0.0002***
Basal versus day 4	ns	ns	ns	0.0022**
Basal versus day 5	ns	ns	ns	ns
Day 1 versus day 2	0.0002***	<0.0001****	ns	0.0008***
Day 1 versus day 3	<0.0001 ****	<0.0001 ****	0.0043 **	0.0001***
Day 1 versus day 4	<0.0001 ****	<0.0001 ****	ns	<0.0001 ****
Day 1 versus day 5	<0.0001****	<0.0001****	0.0449*	<0.0001****
Day 2 versus day 3	ns	ns	ns	ns
Day 2 versus day 4	ns	ns	ns	ns
Day 2 versus day 5	ns	ns	ns	ns
Day 3 versus day 4	ns	ns	ns	ns
Day 3 versus day 5	ns	ns	ns	ns
Day 4 versus day 5	ns	ns	ns	ns

Asterisks summarize the level of significance
ns not significant

with Fig. 10.4 panel A—Tables 10.2 and 10.4, respectively, for detailed statistics). Indeed, LAM significantly increases the day after the end of the primary insult in rats (Fig. 10.2 panel A, $P < 0.0001$, as compared to basal and the following days of epileptogenesis), but significantly decreases in mice (Fig. 10.4 panel A, $P = 0.001$, as compared to the following days of epileptogenesis, no basal condition available). However, it is necessary to consider that when the RAD is a variable and the REC is a fixed parameter, the values of DET and LAM, per se, cannot correlate with the actual amount of determinism and laminarity of the time-series, because the RAD, although variable, can change only under the constrain to reach the imposed fixed amount of recurrences. This may underestimate/overestimate the actual amount of DET and LAM of the time-series. However, the values of DET and LAM calculated considering a small value of the RAD are necessarily the expression of a greater content of determinism and laminarity respect to the same values calculated for a large value of the RAD, since the lower the value of the RAD, the higher the density of trajectories. Therefore, when the RAD is a variable, the actual content of
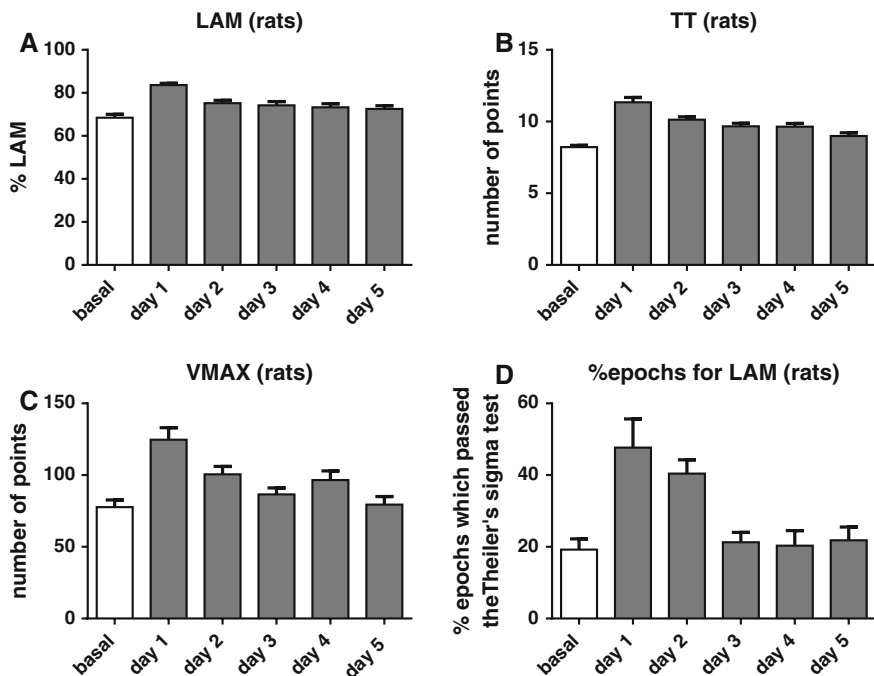
Fig. 10.2 Histograms (mean ± SEM) of datasets of RQA variables calculated in basal condition (*white bar*) and during the early 5 days of epileptogenesis (*grey bars*) for the model of SE induced in rats by the electrical stimulation of the hippocampus. *Panels A*, *B* and *C*, depict how RQA metrics based on the *vertical lines* of the RPs (LAM, TT and VMAX) are affected by the progression of epileptogenesis after the end of the primary insult. *Panel D* reports the percentage of epochs which passed the Theiler's sigma test for the RQA variable LAM during the early phases of epileptogenesis

determinism and laminarity of the time-series can be estimated by the ratios DET/RAD and LAM/RAD. Accordingly, the higher the ratios, the higher the amount of DET and LAM in the time-series. This normalization is equivalent to say that, in our context, if the RAD had been constant as it occurs in the classical RQA, the fraction of recurrent points which form diagonal/vertical lines (i.e., DET and LAM) would be greater for phase spaces with high densities of trajectories, because a fixed RAD would include a greater number of recurrent points.

The normalization of variables DET and LAM respect to the variable RAD immediately shows that the opposite trends of variation of LAM were only apparent. Indeed, the normalization of the variables DET and LAM, highlights how the early 1–2 days of epileptogenesis are characterized by a marked increase of determinism (for rats, Fig. 10.5 panel A, P < 0.0001; for mice, Fig. 10.5 panel C, P < 0.0001—the detailed statistics are reported in Table 10.5) and laminarity (for rats, Fig. 10.5 panel B, P < 0.0001; for mice, Fig. 10.5 panel D, P < 0.0001—see
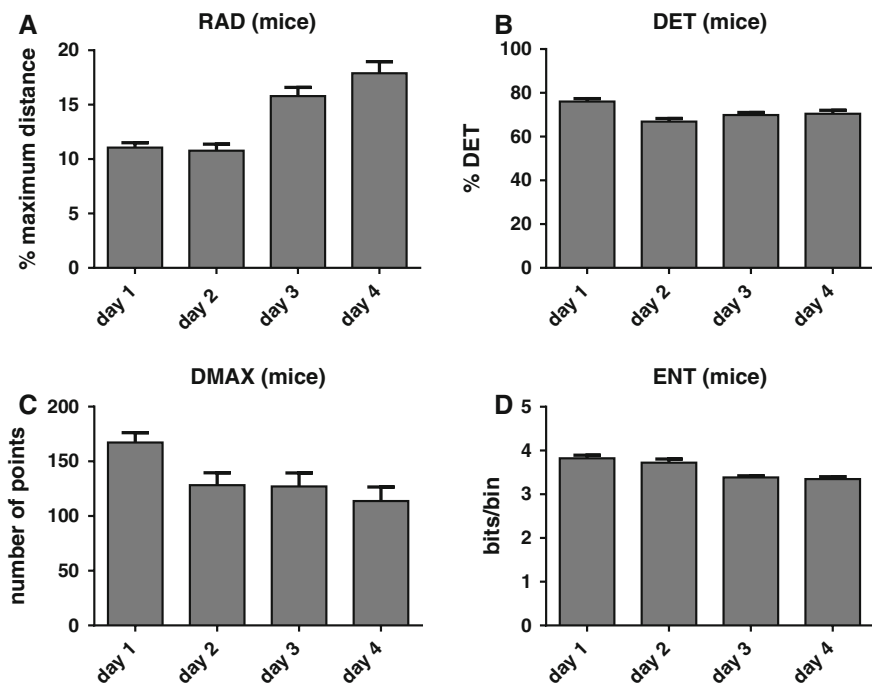
Fig. 10.3 Histograms (mean ± SEM) of datasets of RQA variables calculated during the early 4 days of epileptogenesis for the model of SE induced in mice by the intra-amygdala administration of kainic-acid. *Panel A* depicts the variation of the variable RAD, whereas *panels B*, *C* and *D* show how RQA metrics based on the *diagonal lines* of the RPs (DET, DMAX and ENT) are affected by the progression of epileptogenesis after the end of the primary insult

Table 10.5 for the detailed statistics) in the EEG dynamics which emerge after the end of the SE, a feature occurring in both models of epileptogenesis.

Not only the amount of determinism and laminarity are markedly increased following the end of the SE but, generally, all RQA variables show a significant increase in the early 1–2 days of the latent period. Indeed, this occurred for RQA metrics based on the diagonal line lengths (DMAX), and their related distributions (ENT) (for rats, Fig. 10.1 panels C and D, $P = 0.0039$ and $P < 0.0001$ respectively; for mice, Fig. 10.3 panels C and D, $P = 0.0101$ and $P < 0.0001$ respectively—the detailed statistics for these metrics are reported in Table 10.1 for rats and Table 10.3 for mice) as well as for metrics based on vertical line lengths, as the TT (for rats, Fig. 10.2 panel B, $P < 0.0001$—Table 10.2 for statistics; for mice, Fig. 10.4 panel B, $P = 0.0053$—Table 10.4 for statistics) and the VMAX (for rats, Fig. 10.2 panel C, $P < 0.0001$—Table 10.2 for statistics; for mice, Fig. 10.4 panel C, $P < 0.0001$—Table 10.4 for statistics).
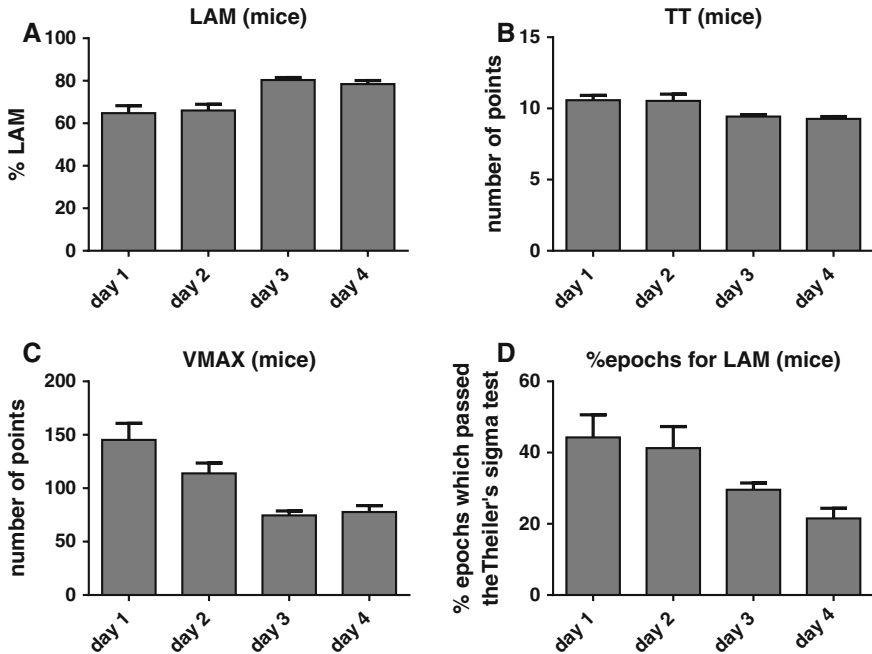
Fig. 10.4 Histograms (mean ± SEM) of datasets of RQA variables calculated during the early 4 days of epileptogenesis for the model of SE induced in mice by the intra-amygdala administration of kainic-acid. *Panels A, B* and *C*, depict how RQA metrics based on the *vertical lines* of the RPs (LAM, TT and VMAX) are affected by the progression of epileptogenesis after the end of the primary insult. *Panel D* reports the percentage of epochs which passed the Theiler's sigma test for the RQA variable LAM

Since the variation of the variable LAM gives a significant hint of the nature of the underlying dynamics, we also calculated the percentage of EEG epochs which passed the TS test for this variable. This metric depicts the probability of the occurrence of a laminar state in the time interval 1:00 pm–7:00 pm depending on the day of the epileptogenesis considered, i.e., how often this dynamic state emerges in function of the day of progression of the epileptogenesis. Not surprisingly, the early 1–2 days are those significantly affected by the highest percentage of occurrence of EEG epochs with significant values of the variable LAM (for rats, Fig. 10.2 panel D, P = 0.0004—statistics in Table 10.2; for mice, Fig. 10.4 panel D, P = 0.0078—statistics in Table 10.4), thus denoting a general persistent condition which is characterized by a high rate of laminarity states within the EEG epochs, i.e., high values of the variable LAM (Fig. 10.5 panels B and D, for rats and mice, respectively), with the additional evidence that this condition repeats frequently, i.e., high percentages of occurrence of EEG epochs which passed the TS test (Fig. 10.2 panel D, for rats; Fig. 10.4 panel D, for mice).

Table 10.2 Nonparametric statistics (Kruskal-Wallis test, followed by Dunn's multiple comparisons test) of RQA metrics reported in Fig. 10.2

	LAM	TT	VMAX	% epochs LAM
Kruskal-Wallis test				
P value	<0.0001****	<0.0001****	<0.0001****	0.0004***
No of groups	6	6	6	6
No of values (total)	307	352	186	41
Kruskal-Wallis statistic	66.94	82.44	35.35	22.67
Dunn's multiple comparisons test				
Groups	*P value*	*P value*	*P value*	*P value*
Basal versus day 1	<0.0001****	<0.0001****	<0.0001****	0.0168*
Basal versus day 2	0.0037**	<0.0001****	0.0159*	0.023*
Basal versus day 3	ns	<0.0001****	ns	ns
Basal versus day 4	ns	<0.0001****	ns	ns
Basal versus day 5	ns	ns	ns	ns
Day 1 versus day 2	0.0001***	ns	ns	ns
Day 1 versus day 3	<0.0001****	0.0116*	0.0017**	0.0434*
Day 1 versus day 4	<0.0001****	0.0014**	ns	ns
Day 1 versus day 5	<0.0001****	<0.0001****	0.0002***	ns
Day 2 versus day 3	ns	ns	ns	ns
Day 2 versus day 4	ns	ns	ns	ns
Day 2 versus day 5	ns	0.0451*	ns	ns
Day 3 versus day 4	ns	ns	ns	ns
Day 3 versus day 5	ns	ns	ns	ns
Day 4 versus day 5	ns	ns	ns	ns

Asterisks summarize the level of significance
ns not significant

Table 10.3 Nonparametric statistics (Kruskal-Wallis test, followed by Dunn's multiple comparisons test) of RQA metrics reported in Fig. 10.3

	RAD	DET	DMAX	ENT
Kruskal-Wallis test				
P value	<0.0001****	0.0006***	0.0101*	<0.0001****
No of groups	4	4	4	4
No of values (total)	184	208	76	259
Kruskal-Wallis statistic	44.23	17.36	11.33	32.62
Dunn's multiple comparisons test				
Groups	*P value*	*P value*	*P value*	*P value*
Day 1 versus day 2	ns	0.0002***	ns	0.024*
Day 1 versus day 3	0.0002***	0.0098**	ns	<0.0001****
Day 1 versus day 4	<0.0001****	ns	ns	<0.0001****
Day 2 versus day 3	<0.0001****	ns	ns	ns
Day 2 versus day 4	<0.0001****	ns	ns	ns
Day 3 versus day 4	ns	ns	ns	ns

Asterisks summarize the level of significance
ns not significant

Table 10.4 Nonparametric statistics (Kruskal-Wallis test, followed by Dunn's multiple comparisons test) of RQA metrics reported in Fig. 10.4

	LAM	TT	VMAX	% epochs LAM
Kruskal-Wallis test				
P value	0.001**	0.0053**	<0.0001****	0.0078**
No of groups	4	4	4	4
No of values (total)	192	269	92	23
Kruskal-Wallis statistic	16.17	12.72	22.84	11.88
Dunn's multiple comparisons test				
Groups	*P value*	*P value*	*P value*	*P value*
Day 1 versus day 2	ns	ns	ns	ns
Day 1 versus day 3	0.0166*	0.0192*	<0.0001****	ns
Day 1 versus day 4	ns	0.0105*	0.0049**	0.0177*
Day 2 versus day 3	0.0017**	ns	ns	ns
Day 2 versus day 4	ns	ns	ns	0.043*
Day 3 versus day 4	ns	ns	ns	ns

Asterisks summarize the level of significance
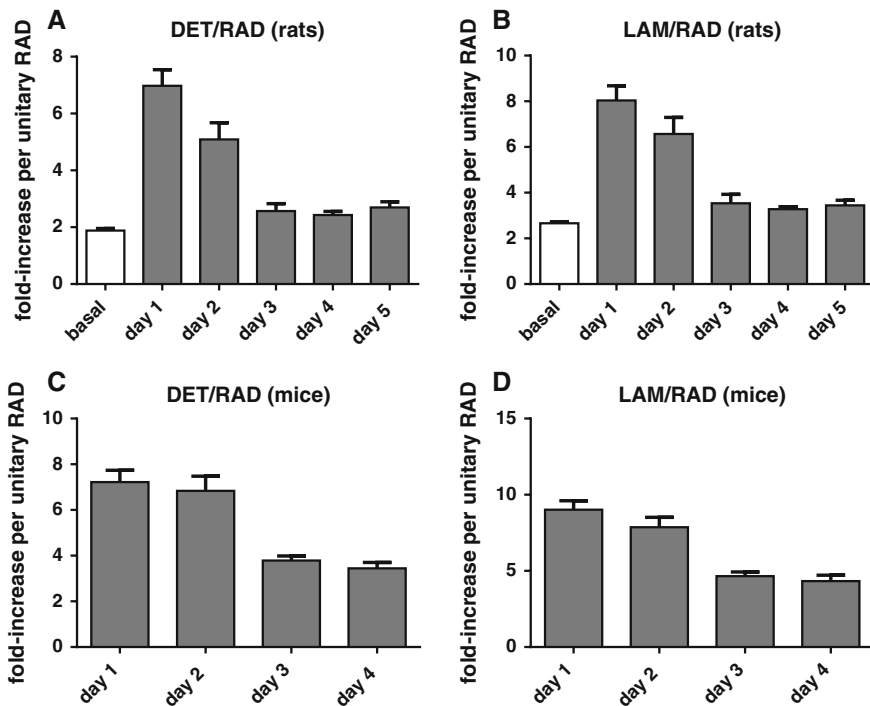*ns* not significant

Fig. 10.5 Histograms (mean ± SEM) of datasets of the RQA variables DET and LAM after their normalization respect to the variable RAD, during the progression of the early phases of epileptogenesis in both models of SE

Table 10.5 Nonparametric statistics (Kruskal-Wallis test, followed by Dunn's multiple comparisons test) of RQA metrics reported in Fig. 10.5

	DET/RAD (rats)	LAM/RAD (rats)	DET/RAD (mice)	LAM/RAD (mice)
Kruskal-Wallis test				
P value	<0.0001****	<0.0001****	<0.0001****	<0.0001****
No of groups	6	6	4	4
No of values (total)	333	303	208	165
Kruskal-Wallis statistic	153.9	131.1	49.86	50.88
Dunn's multiple comparisons test				
Groups	*P value*	*P value*	*P value*	*P value*
Basal versus day 1	<0.0001****	<0.0001****	na	na
Basal versus day 2	<0.0001****	<0.0001****	na	na
Basal versus day 3	ns	0.0364*	na	na
basal versus day 4	ns	0.0166*	na	na
Basal versus day 5	0.0135*	ns	na	na
Day 1 versus day 2	<0.0001****	0.0003***	ns	ns
Day 1 versus day 3	<0.0001****	<0.0001****	<0.0001****	<0.0001****
Day 1 versus day 4	<0.0001****	<0.0001****	<0.0001****	<0.0001****
day 1 versus day 5	<0.0001****	<0.0001****	na	ns
Day 2 versus day 3	0.0002***	0.0108*	0.0003***	0.0007***
Day 2 versus day 4	0.0005***	0.0117*	<0.0001****	0.0002***
Day 2 versus day 5	ns	ns	na	ns
Day 3 versus day 4	ns	ns	ns	ns
Day 3 versus day 5	ns	ns	na	ns
Day 4 versus day 5	ns	ns	na	ns

Asterisks summarize the level of significance
ns not significant

10.4 Discussion

In this study we applied for the first time the RQA to investigate on the nature of EEG dynamics during the early phases of epileptogenesis, thus extending the application of the RQA to the characterization of important models of epileptogenesis in the context of the pre-clinical research in epilepsy. In particular, we deepened the nature of the dynamics involved in the early crucial phases of epileptogenesis elicited by the experimental models of SE.

In the following, we refer to the values of variables DET and LAM after their normalization versus the variable RAD.

For a meaningful evaluation of the nature of the dynamics subtending EEG activity following the end of a pro-epileptogenic primary insult as the SE, we considered the variations of all the RQA metrics based on diagonal and vertical

lines of RPs. At a first sight, the marked increases of ENT, DMAX and DET in the early 1–2 days post-SE may appear contradictory, since a greater degree of complexity (i.e. a wider distribution of diagonal line lengths, hence a higher ENT) usually implies an increase of the exponential instability, normally associated to a decrease of the variables DMAX and DET. Indeed, the DMAX is inversely related to the Lyapunov exponents, and the DET is a measure of the degree of predictability of the system. Nonetheless, the values of both these variables significantly increase.

However, when one takes into account also recurrence measures based on the vertical lines of RPs, it is immediate to notice that also the variables LAM, TT and VMAX significantly increase in the same post-SE temporal window. Altogether, the variations of these variables converge to point out the existence of bifurcation points which subtend a specific non-linear behavior known as intermittency, a dynamical state in which periods of apparent periodicity alternate irregularly with periods which show dynamics driven by the emergence of one or more different attractors, maybe of chaotic nature [23]. We did not determined the type of intermittency. However, this will be done in the near future, also considering an interesting application of the RQA in this context [35]. Intermittency may account for the broad variability of the DMAX, hence the reason for which the statistics related to the DMAX for both models of the SE, are those showing the highest P values (according to the Kruskal-Wallis test), as also the lack of statistical significances (according to the Dunn's post hoc test) for the same variable calculated from the EEG epochs of mice (Fig. 10.3 panel C).

The episodes of intermittency in the early latent period are not only more accentuated but, generally, they occur much more frequently, as evinced by the significantly high percentage of EEG epochs which passed the TS test for LAM. Therefore, the early post-SE days are affected by long-lasting temporal windows characterized by persistent instability of intermittency type. This condition appears as a general feature of the early phases of epileptogenesis triggered by SE, since we investigated two different models of SE, yielding similar results.

In the context of the epilepsy research, the occurrence of intermittency as dynamical regime is not a novelty since it was shown to emerge during ictal activities in epileptic patients or in rodents during the progression of the SE [36, 37]. However, our study shows that intermittency regimes persist beyond the end of the SE even without the occurrence of ictal events and emerge at high rates in the early days following the end of the primary insult.

It is of interest to notice that also without the emergence of typical widespread ictal activities, ictogenic brain areas are characterized by a high rate of occurrence of spatially distributed micro-seizures [41]. Since the intermittency may characterize the dynamics of ictal events [37], the emergence of intermittency regimes in the early phases of epileptogenesis could be the expression of such micro-seizures originating from an epileptogenic network under formation, due to the occurrence of neurodegenerative phenomena and functional alterations affecting the early phases of epileptogenesis following the end of the SE [38–40]. From this perspective, one also notices that our data show a general descending trend of the RQA

variables after day 2 post-SE, likely due to a progressive weakening of the contribution of nonlinear dynamics to the EEG signal detected by the measuring electrode. Interestingly, this descending trend could be compatible with the formation of topographically distributed ictogenic micro-domains, as a consequence of the progression of epileptogenesis [41, 42].

In authors' opinion, it is also of interest to notice that the percentage of epochs passing the TS test for the variable LAM in basal conditions (Fig. 10.2 panel D) is not negligible, thus suggesting that the intermittency could be a dynamical state which may occur also without an overt pathology. This finding is consistent with evidence of occurrence of micro-seizures also in basal conditions, as it was shown in healthy humans [41]. Altogether, our findings could reasonably support the hypothesis that the main aberrant feature of ictal events is not their nonlinear dynamical nature, but their spreading over an abnormally extended spatio-temporal scale, as proposed also by other investigators [41, 42].

Since it is reasonable to hypothesize that the emergence of intermittency could be the dynamic hallmark of pro-epileptogenic insults and could correlate with the efficacy of such insults to promote functional changes leading to the development of epilepsy, an important future work will be to establish the existence (if any) of a relationship between pro-epileptogenic insults and the emergence of such dynamics. To this aim, the same therapeutic interventions which were shown able to prevent/modify the development of epilepsy can be used, and this study could lead to (i) the identification of the emergence of intermittency as a potential prognostic factor of the development of epilepsy and (ii) a significant improvement of the portability of pre-clinical studies aimed to test new potential therapeutics able to prevent the development of epilepsy. From this perspective, it is worth considering that, nowadays, the direct comparison of results obtained in different models of SE is often impaired. Indeed, metrics which are commonly used to evaluate the efficacy of potential therapeutics in the experimental models (e.g., the number of spikes per hour) are based on the EEG patterns intrinsically associated to the progression of the prolonged ictal activity of the SE. However, these patterns of EEG activity are remarkably model-dependent. Therefore, it is often hard to compare experimental results from different models, when considering these metrics. However, despite the remarkable differences between the two models of SE that we investigated, we clearly show that the enhanced and persistent rate of occurrence of laminarity states in the EEG dynamics during the early days of epileptogenesis is a common feature of both models. This suggests that such dynamic behaviour could be model-independent and could be a better metric to validate results obtained from the application of potential therapeutics using different models of epileptogenesis, thus improving the portability of pre-clinical studies.

usage of Grid Computing resources and services provided by the Italian Grid Infrastructure (IGI, http://www.italiangrid.it/).

Conflict of Interest Authors have no conflict of interest to declare.

References

1. A. Pitkänen, K. Lukasiuk, Molecular and cellular basis of epileptogenesis in symptomatic epilepsy. Epil. Behav. **14**(1), 16–25 (2009)
2. A. Pitkänen, K. Lukasiuk, Mechanisms of epileptogenesis and potential treatment targets. Lancet Neurol. **10**(2), 173–186 (2011)
3. C.L. Webber, J.P. Zbilut, Dynamical assessment of physiological systems and states using recurrence plot strategies. J. Appl. Physiol. **76**(2), 965–973 (1994)
4. J.P. Zbilut, A. Giuliani, C.L. Webber, Detecting deterministic signals in exceptionally noisy environments using cross-recurrence quantification. Phys. Lett. A **246**(1), 122–128 (1998)
5. J.P. Zbilut, A. Giuliani, C.L. Webber, Recurrence quantification analysis as an empirical test to distinguish relatively short deterministic versus random number series. Phys. Lett. A **267**(2), 174–178 (2000)
6. W. Löscher, C. Brandt, Prevention or modification of epileptogenesis after brain insults: experimental approaches and translational research. Pharmacol. Rev. **62**(4), 668–700 (2010)
7. A. Pitkänen, Therapeutic approaches to epileptogenesis—hope on the horizon. Epilepsia **51**(s3), 2–17 (2010)
8. D.H. Lowenstein, B.K. Alldredge, Status epilepticus. N. Engl. J. Med. **338**(14), 970–976 (1998)
9. A. Pitkänen, I. Kharatishvili, S. Narkilahti, K. Lukasiuk, J. Nissinen, Administration of diazepam during status epilepticus reduces development and severity of epilepsy in rat. Epil. Res. **63**(1), 27–42 (2005)
10. M.J. Lehmkuhle, K.E. Thomson, P. Scheerlinck, W. Pouliot, B. Greger, F.E. Dudek, A simple quantitative method for analyzing electrographic status epilepticus in rats. J. Neurophysiol. **101**(3), 1660–1670 (2009)
11. M.G. De Simoni, C. Perego, T. Ravizza, D. Moneta, M. Conti, F. Marchesi, A. De Luigi, S. Garattini, A. Vezzani, Inflammatory cytokines and related genes are induced in the rat hippocampus by limbic status epilepticus. Eur. J. Neurosci. **12**(7), 2623–2633 (2000)
12. F. Noè, A.H. Pool, J. Nissinen, M. Gobbi, R. Bland, M. Rizzi, C. Balducci, F. Ferraguti, G. Sperk, M.J. During, A. Pitkänen, A. Vezzani, Neuropeptide Y gene therapy decreases chronic spontaneous seizures in a rat model of temporal lobe epilepsy. Brain **131**(6), 1506–1515 (2008)
13. G. Mouri, E. Jimenez-Mateos, T. Engel, M. Dunleavy, S. Hatazaki, A. Paucard, S. Matsushima, W. Taki, D.C. Henshall, Unilateral hippocampal CA3-predominant damage and short latency epileptogenesis after intra-amygdala microinjection of kainic acid in mice. Brain Res. **1213**, 140–151 (2008)
14. E.M. Jimenez-Mateos, T. Engel, P. Merino-Serrais, R.C. McKiernan, K. Tanaka, G. Mouri, T. Sano, C. O'Tuathaigh, J. Waddington, S. Prenter, N. Delanty, M.A. Farrell, D.F. O'Brien, M. R. Conroy, R.L. Stallings, J. deFelipe, D.C. Henshall, Silencing microRNA-134 produces neuroprotective and prolonged seizure-suppressive effects. Nat. Med. **18**(7), 1087–1094 (2012)
15. G. Paxinos, C. Watson, *The Rat Brain in Stereotaxic Coordinates* (Academic Press, New York, 2005)
16. K.B.J. Franklin, G. Paxinos, *The Mouse Brain in Stereotaxic Coordinates* (Academic Press, San Diego, 2008)

17. F. Frigerio, A. Frasca, I. Weissberg, S. Parrella, A. Friedman, A. Vezzani, F.M. Noe, Long-lasting pro-ictogenic effects induced in vivo by rat brain exposure to serum albumin in the absence of concomitant pathology. Epilepsia **53**(11), 1887–1897 (2012)
18. L. Chauvière, N. Rafrafi, C. Thinus-Blanc, F. Bartolomei, M. Esclapez, C. Bernard, Early deficits in spatial memory and theta rhythm in experimental temporal lobe epilepsy. J. Neurosci. **29**(17), 5402–5410 (2009)
19. J. Seo, S. Jung, S.Y. Lee, H. Yang, B.S. Kim, J. Choi, M. Bang, H.S. Shin, D. Jeon, Early deficits in social behavior and cortical rhythms in pilocarpine-induced mouse model of temporal lobe epilepsy. Exp. Neurol. **241**, 38–44 (2013)
20. H. Poincaré, Sur le problème des trois corps et les équations de la dynamique. Acta Math. **13**(1), A3–A270 (1890)
21. J.P. Eckmann, S.O. Kamphorst, D. Ruelle, Recurrence plots of dynamical systems. Europhys. Lett. **4**(9), 973 (1987)
22. N. Marwan, Encounters with neighbours: current developments of concepts based on recurrence plots and their applications. Ph.D. Thesis, University of Potsdam (2003)
23. N. Marwan, M. Carmen Romano, M. Thiel, J. Kurths, Recurrence plots for the analysis of complex systems. Phys. Rep. **438**(5), 237–329 (2007)
24. F. Takens, Detecting strange attractors in turbulence, in *Dynamical Systems and Turbulence*, Warwick 1980 (Springer, Berlin, 1981), pp. 366–381
25. C.L. Webber, J.P. Zbilut, Recurrence quantification analysis of nonlinear dynamical systems. in *Tutorials in Contemporary Nonlinear Methods for the Behavioral Sciences*, ed. by M.A. Riley, G.C. Van Orden, pp. 26–94 (2005). http://www.nsf.gov/sbe/bcs/pac/nmbs/chap2.pdf
26. J. Theiler, S. Eubank, A. Longtin, B. Galdrikian, Farmer J. Doyne, Testing for nonlinearity in time series: the method of surrogate data. Physica D **58**(1), 77–94 (1992)
27. J. Gao, Z. Zheng, Direct dynamical test for deterministic chaos and optimal embedding of a chaotic time series. Phys. Rev. E **49**(5), 3807 (1994)
28. M. Thiel, M.C. Romano, J. Kurths, R. Meucci, E. Allaria, F.T. Arecchi, Influence of observational noise on the recurrence quantification analysis. Physica D **171**(3), 138–152 (2002)
29. T. Schreiber, A. Schmitz, Surrogate time series. Physica D **142**(3), 346–382 (2000)
30. G. Ouyang, X. Li, C. Dang, D.A. Richards, Using recurrence plot for determinism analysis of EEG recordings in genetic absence epilepsy rats. Clin. Neurophysiol. **119**(8), 1747–1755 (2008)
31. T. Schreiber, A. Schmitz, Improved surrogate data for nonlinearity tests. Phys. Rev. Lett. **77**(4), 635 (1996)
32. R. Barbera, G. La Rocca, M. Rizzi, Grid computing technology and the recurrence quantification analysis to predict seizure occurrence in patients affected by drug-resistant epilepsy, in *Data Driven e-Science* (Springer, New York, 2011), pp. 493–506
33. C.L. Webber, Introduction to recurrence quantification analysis RQA version 13.1 README. PDF. http://homepages.luc.edu/~cwebber/RQA131.EXE
34. R. Hegger, H. Kantz, T. Schreiber, Practical implementation of nonlinear time series methods: the TISEAN package. Chaos **9**(2), 413–435 (1999)
35. K. Klimaszewska, J.J. Żebrowski, Detection of the type of intermittency using characteristic patterns in recurrence plots. Phys. Rev. E **80**(2), 026214 (2009)
36. J.L. Velazquez, H. Khosravani, A. Lozano, B. Bardakjian, P.L. Carlen, R. Wennberg, Type III intermittency in human partial epilepsy. Eur. J. Neurosci. **11**(7), 2571–2576 (1999)
37. J.L.P. Velazquez, M.A. Cortez, O.C. Snead, R. Wennberg, Dynamical regimes underlying epileptiform events: role of instabilities and bifurcations in brain activity. Physica D **186**(3), 205–220 (2003)
38. J.A. Gorter, P.M.G. Pereira, E.A. Van Vliet, E. Aronica, F.H.L. Da Silva, P.J. Lucassen, Neuronal cell death in a rat model for mesial temporal lobe epilepsy is induced by the initial status epilepticus and not by later repeated spontaneous seizures. Epilepsia **44**(5), 647–658 (2003)

39. T. Araki, R.P. Simon, W. Taki, J.Q. Lan, D.C. Henshall, Characterization of neuronal death induced by focally evoked limbic seizures in the C57BL/6 mouse. J. Neurosci. Res. **69**(5), 614–621 (2002)

40. A. Vezzani, M. Conti, A. De Luigi, T. Ravizza, D. Moneta, F. Marchesi, M.G. De Simoni, Interleukin-1β immunoreactivity and microglia are enhanced in the rat hippocampus by focal kainic-acid application: functional evidence for enhancement of electrographic seizures. J. Neurosci. **19**(12), 5054–5065 (1999)

41. M. Stead, M. Bower, B.H. Brinkmann, K. Lee, W.R. Marsh, F.B. Meyer, B. Litt, J. Van Gompel, G.A. Worrell, Microseizures and the spatiotemporal scales of human partial epilepsy. Brain **133**, 2789–2797 (2010)

42. A. Bragin, C.L. Wilson, J. Engel, Chronic epileptogenesis requires development of a network of pathologically interconnected neuron clusters: a hypothesis. Epilepsia **41**(s6), S144–S152 (2000)